CONF-901116--13

Angular Distributions of Single- and Double-Electron Capture in Very-Slow Ar^{6+}–Ar Collisions

CONF-901116--13

DE91 001217

C. Biedermann, J.C. Levin, R.T. Short, S.B. Elston, J.P. Gibbons, K. Kimura, N. Keller and I.A. Sellin

Department of Physics, University of Tennessee, Knoxville, Tennessee 37996-1200 and Oak Ridge National Laboratory, Oak Ridge, Tennessee 37831-6377

H. Cederquist, L.R. Andersson, H. Andersson and L. Liljeby

Manne Siegbahn Institute of Physics, S-10405 Stockholm, Sweden

PACS number(s): 34.70.+e, 34.50.Fa

Abstract

We have measured state-resolved angular distributions of one- and two-electron capture in 32 to 800 *eV* $Ar^{6+} - Ar$ collisions. The experimental energy-gain spectra show that single-electron capture mainly populates the $5s$, $5p$ and $4f$ levels. We observe detailed structures in the corresponding angular distributions, but a final interpretation has to await a quantitative analysis of the collision dynamics. We tentatively ascribe the main features in the angular distribution of true double-electron capture at Q~26 eV ($4s4f$ and $4s5s$) and Q~42 eV ($3d4d$) to processes involving two consecutive one-electron transitions. For the transfer ionization process, we measure a Q-value of ~26 eV, which we assign to autoionizing $4s5s$ (or $4s4f$) levels. The $4s5s$, $4s4f$, and $3d4d$ levels all reside above the first ionization limit of Ar^{4+}, but we find that the $3d4d$ level stabilizes through radiative decay.

1 Introduction

The field of electron capture by slow multiply charged projectile ions has attracted extensive attention in recent years [1]. This is driven by the need for experimental and theoretical information on charge-exchange mechanisms in laboratory and astrophysical plasmas and the rapid development of sources for high-charge-state ions with low kinetic energies.

At low collision velocities (when the relative velocity between the projectile and the target is much smaller than the orbital velocities of the active electrons) the process of state-selective electron capture can be described within a quasimolecular picture. In many of these cases electron transfer takes place near well-localized avoided crossings between adiabatic potential energy curves of the same spin and symmetry. The transition probabilities depend on the energy separations at the avoided crossings. Total and differential cross sections can be calculated using a multichannel Landau-Zener formalism. We have applied this method with considerable success to our recent results for very-slow $Ar^{4+} - Ar$ collisions [2,3]. Here we present experimental results for $Ar^{6+} - Ar$ collisions in the energy range 32 to 800 eV. The analysis of the results is, however, still preliminary.

When the collision energy is lowered, angular-differential cross sections provide more detailed information on the interaction potentials and the dynamics of the collision through resolvable rainbow and interference effects. Additional information on the internal states of the collision products can be obtained by recording the projectile energy gain. With our setup it is possible to obtain simultaneously data on projectile scattering angles and energies. We show results for angular-differential cross sections for transfer

ionization, single-, and double-electron capture for 32 to 800 eV $Ar^{6+} - Ar$ collisions.

2 Experimental technique

In the following we only give a brief summary of the experimental apparatus, since a detailed description can be found in Ref. [2]. A pump beam of 30 MeV Cl^{5+} ions from the Oak Ridge National Laboratory EN-12 tandem Van de Graaff accelerator is post stripped and directed into a gas cell in order to produce recoil ions. Argon recoil ions are first extracted with a small electric field and then accelerated to the potential of a Wien-filter for charge-to-mass separation. After retardation and collimation, the very-slow ion beam crosses an effusive gas-jet target at right angles. All regions of high gas densities are enclosed in differential pump steps in order to minimize charge transfer during the analysis and transport of the very-slow ion beam outside the target region. The beam energy is determined by the charge state and the potential difference between the zone of recoil-ion creation and the collision region held at ground potential. In order to achieve good resolution in the post-collisional energy-gain spectra, the energy spread of the very-slow ion beam is kept at a minimum by the use of low extraction field strengths and tight collimation of the pump beam. After the interaction of the very-slow ion beam with the gas-jet target, the charge states, energies and scattering angles are analyzed by a 64° cylindrical electrostatic analyzer and a multichannel plate with a two-dimensional position-sensitive anode. Since the analyzer focusses only in one dimension, energy-gain values are obtained from the position recorded along the direction of energy dispersion,

while scattering angles are derived from the vertical position on the detector and the trajectory length between the interaction region and the detector. The relative energy resolution is about 1.6 %. The angular divergence of the very-slow beam was measured to be $\pm 0.5°$ and the acceptance angle is limited to $\pm 9°$ by the diameter of the position-sensitive detector.

3 Results and discussion

In fig. 1 we show angular distributions for single-electron capture in Ar^{6+} on Ar collisions at 32 (a), 59 (b), 97 (c) and 199 eV (d). In the corresponding energy-gain spectra we observe that single-electron capture mainly populates the $5s$ state of Ar^{5+} with smaller contributions of the $5p$ and $4f$ levels, which are close in excitation energy. These observations are in accordance with the findings in higher resolution energy-gain experiments of Nielsen et al. [4] and Giese et al. [5] at higher projectile energies. The former authors found that the cross section for capture to the $5s$ level is about 3 times larger than the cross section for $5p$ and $4f$ at 100 eV [4]. The relative populations of the $5s$ and $5p$ levels increase when the velocity is lowered. This shift in intensity is expected since the reaction window, which indicates the favored final states, shifts towards larger internuclear distance with decreasing energy.

Fig. 2 shows the potential energy curve diagram for the collision system as a function of the internuclear distance R. In a first approximation the potential energy for the incoming channel $Ar^{6+}\ 3s^2 + Ar\ 3p^6$ is taken to be flat. The four relevant outgoing single-capture channels $Ar^{5+}\ 3s^2\ nl + Ar^{+}\ 3p^5$ and two double-capture channels $Ar^{4+}\ 3s^2\ nl\,n'l' + Ar^{2+}\ 3p^4$ are dominated by the Coulomb interaction, from which the inelasticity of

the reaction for the respective final state is subtracted. The crossings of the diabatic potential curves with the $5p$, the $5s$ and the $4f$ channels lie fairly well separated at the internuclear distances of 16, 11.5 and 9 $a.u.$, respectively.

We have indicated estimates of scattering angles for the capture to the $5p$, $5s$ and $4f$ states (from left to right) for each of the angular distributions shown in fig. 1. The estimates are arrived at by assuming impact parameters equal to the crossing radii of the populated channels. These half-Coulomb scattering angles θ_c occur where $\frac{db}{d\theta} = 0$ in the classical deflection functions. It is clearly seen in fig. 1 that these estimates by no means represent lower limits for projectile scattering angles θ. This is because the transition may take place on the way out from the collision resulting in smaller deflections. At the two highest energies (fig.1(c) and (d)) the three θ_c lie close to the second maxima, while the inner maxima possibly could be due to rainbow scattering at the repulsive inner wall $4d$ [4]. It is, however, clear that a more detailed analysis involving multichannel Landau-Zener calculations or coupled channel calculations are needed in order to understand even the more prominent features of the angular distributions of single-electron capture.

In the energy-gain spectra for true double-electron capture in fig. 3 (a), two structures corresponding to inelasticities of $Q = 26\ eV$ and $42\ eV$ are observed. The energy-gain peaks are shifted to lower energy values due to the large scattering angles associated with two-electron capture. The Q-values of 26 and 42 eV indicate total binding energies for two electrons captured to Ar^{6+} projectile of 69 and 85 eV respectively. The binding energy of the Ar^{5+} ground state is 91 eV with respect to Ar^{6+}. Binding energies for relevant doubly-excited states are not readily found in tables,

but some information on the structure can be gained by using an extended Rydberg formula given by e.g. Read [6]. Quantum defects of single-electron capture states can be found from energy levels of Ar^{5+} [4,7]. Energy levels of Ar^{4+} with the configuration [core]($4s\ nl$), with $nl = 4f$, $5s$, $5p$ are thus estimated to be in the immediate vicinity of the double-capture channel with $Q = 26\ eV$, whereas configurations like [core]($3d\ nl$) seem to have energies near the $Q = 42\ eV$ double-capture channel. The widths of the two double-electron capture peaks are fairly large due to several close-lying capture levels and kinematic effects.

In fig. 4, the angular distribution of true double-electron capture [(a) dashed line] is compared to the distribution of single-electron capture [(a) solid line] and transfer ionization [(b) dashed line] at 450 eV. In the true double-electron capture process two electrons are transferred between the target and a non-autoionizing projectile state, whereas the transfer ionization process involves the emission of one electron from the projectile. The angular distribution of true double-capture shows a double-peak structure at large scattering angles (3.2 and 4.2°). Estimates of θ_c for direct (one-step) transitions between the initial and final channels result in angles of 1.7 and 2.5° for $Q = 26$ and $Q = 42\ eV$, respectively. Instead, the peak at 3° most probably results from two sequential one-electron transitions: the first one from the initial channel to either the $5s$ or the $4f$ state and the second one from capture of a second electron to the $4s$ state. Doubly-excited $4s4f$ and $4s5s$ states could thus be formed with a Q-value of 26 eV and the corresponding rainbow scattering angles are observed in both the true double-electron capture and transfer ionization spectra at ~3°. The $Q = 42\ eV$ channel which only is seen in the true double-capture spectrum is most likely pop-

ulated through the diabatic $4d$ single-capture channel [4] and its coupling to the $3d4d$ channel (cf. fig. 2). The feature at about 6° is probably due to two-step population of $3d4f$ and/or $3d5s$ levels. Comparing the angular distribution of transfer ionization (b) in fig. 4 with the angular distribution for true double-electron capture (a) we can conclude that the structure at smaller scattering angles of 3° is associated with a Q-value of 26 eV and the larger (4.2°) scattering angles with $Q = 42$ eV. Although both double-capture channels are energetically allowed to decay via autoionization, only transfer ionization states with Q-values close to 26 eV are observed. This is surprising, since one would expect a larger branching ratio for autoionization of $Q = 42$ eV excited states, because this requires the emission of an electron with lower energy than does the process for the $Q = 26$ eV channel. On the other hand, we have seen that states with high angular momentum components probably are populated in the two-electron capture process at $Q = 42$ eV. This might imply a low autoionization rate, due to weak interactions between electrons with high angular momentum. The ratio between the cross sections for true double-capture and transfer ionization is about 1.5 at 450 eV within our angular acceptance. With higher collision energies the angular distributions of single- and double-electron capture move to smaller scattering angles and total capture cross sections have been reported in Ref. [8].

4 Conclusion

We have shown results for state-selective angular distributions for one- and two-electron capture processes in very slow $Ar^{6+} - Ar$ collisions investigated

with an experimental setup utilizing a recoil-ion source for production of an intense, very-slow ion beam of high charge. We record post-collisional scattering angles and projectile energy-gain simultaneously. The structures observed in the angular distributions for single-electron capture are similar to the ones reported for other collision systems at very low energies such as $Ar^{4+} - Ar$ [2] and $Ar^{6+} - He$ [3], which have been found to be dominated by multiple rainbow scattering. The large scattering angles for double-electron capture and transfer ionization are most likely due to a sequential electron-transfer process. We have observed features at 3.2° and 4.2° in the angular distribution of true double-electron capture which we tentatively ascribe to the formation of radiatively stabilizing doubly-excited Ar^{4+} levels of $4s4f$ ($Q \sim 26\ eV$) and $3d4d$ ($Q \sim 42\ eV$), respectively. The strongest peak in the angular distribution of transfer ionization might be $4s5s$ ($Q \sim 26\ eV$), for which preferential of autoionization could be due to strong interaction between the two s electrons.

Acknowledgment

This work was supported in part by the National Science Foundation; the U.S. Department of Energy, Office of Basic Energy Sciences, Division of Chemical Sciences, under Contract No. DE-AC05-84OR21400 with Martin Marietta Energy Systems Inc.; and by the Swedish Natural Science Research Council.

References

[1] R.K. Janev and H. Winter, Phys. Rep. **117** (1985) 265.

[2] C. Biedermann, H. Cederquist, L.R. Andersson, J.C. Levin, R.T. Short, S.B. Elston, J.P. Gibbons, H. Andersson, L.Liljeby, I.A. Sellin, Phys. Rev. **A 41** (1990) 5889.

[3] L.R. Andersson, this conference.

[4] E.H. Nielsen, L.H. Andersen, A. Bárány, H. Cederquist, P. Hvelplund, H. Knudsen, K.B. MacAdam and J. Sørensen, J. Phys. B **17** (1984) L139.

[5] J.P. Giese, C.L. Cocke, W. Waggoner, L.N. Tunnell and S.L. Varghese, Phys. Rev. **A 34** (1986) 3770.

[6] F.H. Read, J. Phys. B **10** (1977) 449.

[7] S. Bashkin and J.O. Stoner, Atomic Energy Levels and Grotrian Diagrams (Amsterdam, North-Holland , 1978).

[8] C. Biedermann, J.C. Levin, R.T. Short, S.B. Elston, J.P. Gibbons, I.A. Sellin, H. Cederquist, L.R. Andersson, H. Andersson, L.Liljeby, Phys. Rev. A, in press (1990).

Figure 1: Angular distributions for single-electron capture in $Ar^{6+} - Ar$ collisions at 32 (a), 59 (b), 97 (c) and 199 eV (d). Indicated by arrows are the estimated scattering angles derived from a half-Coulomb scattering model for capture to the $5p$, $5s$ and $4f$ levels of Ar^{5+} (from left to right). At 32 eV only the estimated angle for $5p$ capture is shown. The horizontal bars mark the FWHM of the incident Ar^{6+} beam profile.

Figure 2: Schematic potential energy diagram for the $Ar^{6+} - Ar$ collision system. The potential energy curves for the incoming channel and the exiting single- and double-electron capture channels are plotted as functions of the internuclear distance R.

Figure 3: Energy-gain spectra for double-electron capture (a) within projectile scattering angles of $5 \pm 2°$, and for single-electron capture (b) within $3 \pm 1.5°$ in 450 eV $Ar^{6+} - Ar$ collisions. The peak structure in (b) at higher energy-gain values corresponds to a Q-value of 26 eV and is due to autoionization in one of the double-capture channels. The horizontal bar indicates the energy resolution of the cylindrical analyzer.

Figure 4: Angular distributions for single-electron capture [(a) solid line], true double-electron capture [(a) dashed line] and transfer ionisation [(b) dashed line] in 450 eV $Ar^{6+} - Ar$ collisions. The intensity of the single-capture peak is reduced by a factor of 10 for clarity. The horizontal bar marks the FWHM of the incident Ar^{6+}-beam profile.

Fig. 1

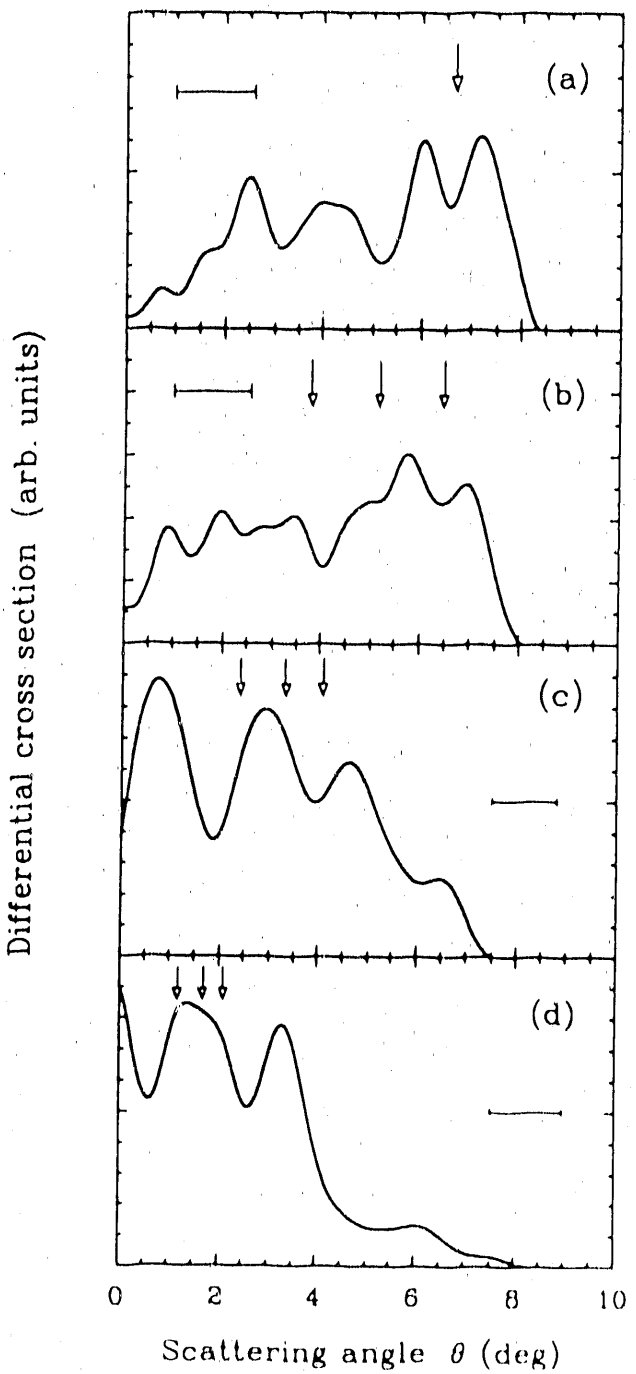
(a)
(b)
(c)
(d)
Differential cross section (arb. units)
0
2
4
6
8
10
Scattering angle θ (deg)

Fig. 2

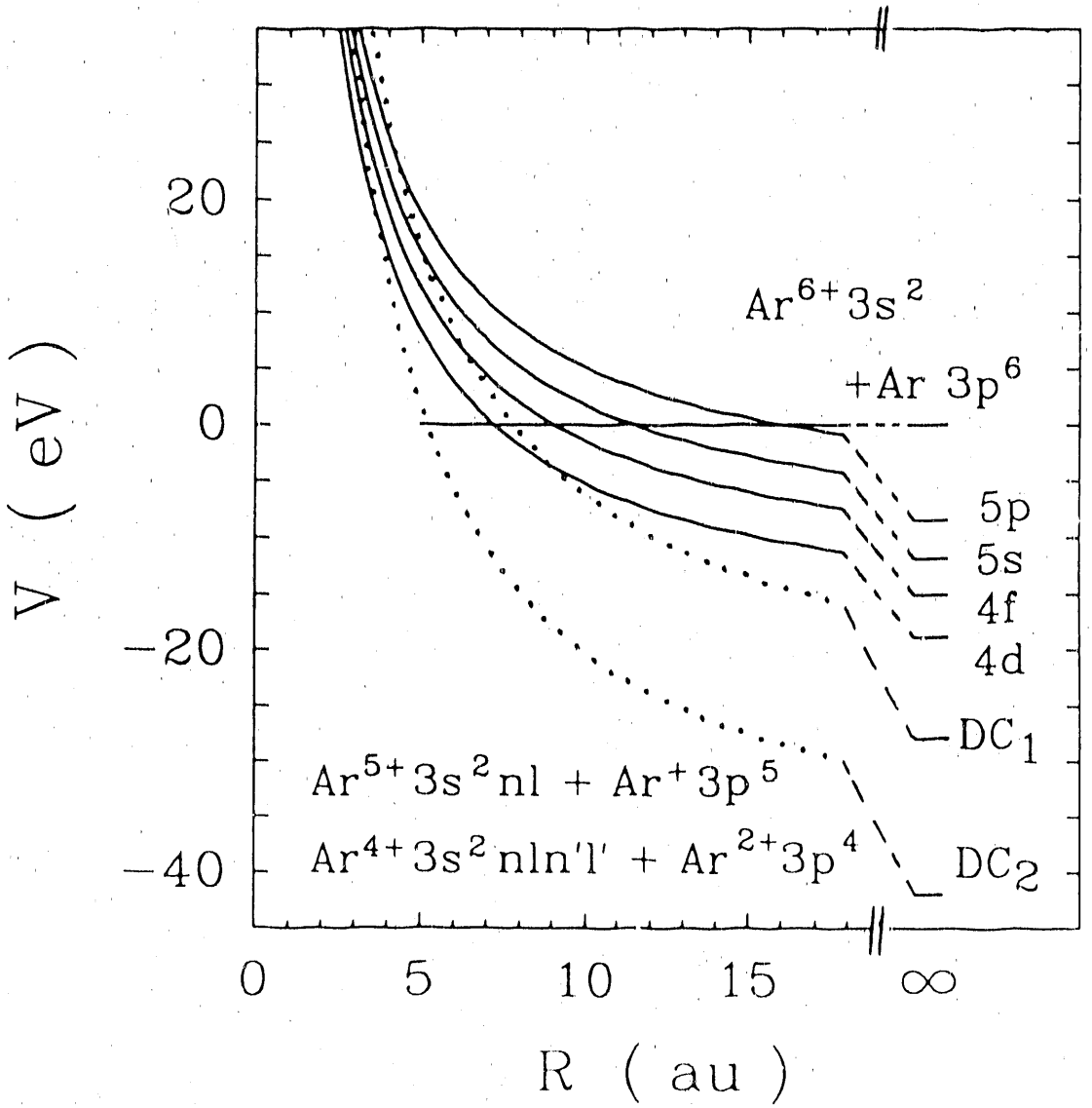
20
0
−20
−40
V (eV)
0
5
10
15
∞
R (au)
$Ar^{6+}3s^2$
$+Ar\ 3p^6$
5p
5s
4f
4d
DC_1
$Ar^{5+}3s^2nl + Ar^{+}3p^5$
$Ar^{4+}3s^2nln'l' + Ar^{2+}3p^4$
DC_2

Fig. 3

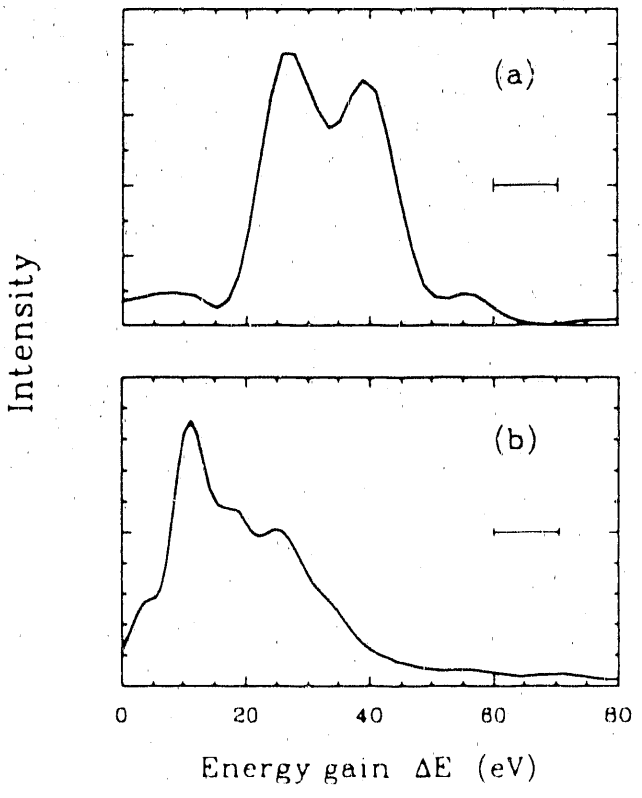

Fig. 4

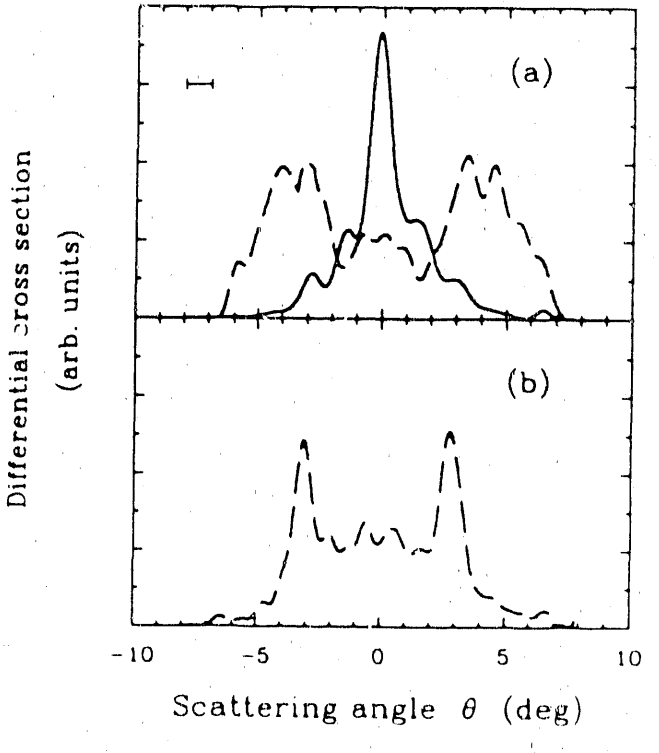
(a)
(b)
Differential cross section
(arb. units)
-10
-5
0
5
10
Scattering angle θ (deg)

END

DATE FILMED

11 / 07 / 90